Design and Performance of a Novel Interference-Free GFDM Transceiver With Dual Filter

Fei Li, *Student Member, IEEE*, Kan Zheng, *Senior Member, IEEE*, Long Zhao, *Member, IEEE*, Hui Zhao, and Yonghui Li, *Fellow, IEEE*

***Abstract*—Generalized frequency division multiplexing (GFDM) as a sub-carrier filtered scheme can flexibly handle various different application scenarios of the fifth-generation system. However, due to the intrinsic self-interference resulting from the filter, the channel estimation becomes very hard, particularly when GFDM works with a multi-input multi-output (MIMO) system. In this paper, a new GFDM-dual filter (GFDM-DF) transmission scheme is proposed, which can guarantee the orthogonality of sub-carriers, so that the intrinsic self-interference can be eliminated. We first divide information symbols into odd-numbered and even-numbered sub-carrier symbols. Then, the orthogonality conditions for GFDM-DF are derived. According to the orthogonality conditions, we choose two different filters for odd-numbered and even-numbered sub-carriers. The signal-to-interference ratio of either the conventional GFDM or GFDM-DF is also evaluated. Moreover, based on the characteristics of the receiving matrix, we further design a low-complexity GFDM-DF receiver. Numerical results show that GFDM-DF can work well with the channel estimation and the MIMO system and its performance is better than that of the conventional GFDM system.**

***Index Terms*—Multi-carrier, GFDM, pilot, MIMO, dual-filter.**

I. Introduction

ORTHOGONAL frequency division multiplexing (OFDM) has been widely used as the baseline waveform in modern communication systems, such as WiFi and cellular networks [2]. The main benefits of OFDM are the use of cyclic prefix (CP) to eliminate the inter-symbol interference [3], [4], and simple receiver based on the fast Fourier transformation (FFT) [5], [6]. However, OFDM also affected by some disadvantages, such as the spectrum inefficiency caused by the excessive CP and the large sidelobe resulting from the rectangular pulse. In addition, strict synchronization is required to keep orthogonality between sub-carriers [7], [8].

In order to deal with the shortcomings of OFDM, new multi-carrier technologies such as generalized frequency division multiplexing (GFDM) [9] have recently been paid much attention. GFDM is a block-based multi-carrier modulation system. To reduce the filter tails, a cyclic pulse shaping filter is employed. The OOB radiation of GFDM becomes very small due to the introduction of an adjustable filter [10]. This significantly reduces the OOB interference, which greatly benefits the dynamic spectrum access scenario. Besides, GFDM also can be designed as a generalized multi-carrier scheme with both OFDM to single carrier as its special cases [11]. Only one CP is used in a GFDM block, which greatly improves the spectral efficiency and benefits the low latency. Moreover, GFDM can also meet the demand of low latency by reducing the symbol duration. Finally, GFDM can be regarded as a kind of single-carrier transmission, which can alleviate the PAPR performance. However, GFDM also has its drawbacks. Because the usage of pulse shaping filter, the sub-carriers become non-orthogonality and some intrinsic self-interference emerged, e.g., inter-carrier interference (ICI) and inter-symbol interference (ISI) [12]. The intrinsic self-interference not only degrades the demodulation performance of GFDM system but also makes the channel estimation (CE) and multiple-input multiple-output (MIMO) complex.

In order to improve these deficiencies, some linear receivers can be used, such as zero-forcing (ZF) and minimum mean square error (MMSE). However, the noise might be amplified by the ZF receiver, while the MMSE receiver has high computational complexity. GFDM with successive interference cancellation (SIC) is proposed in [13], but the complexity of GFDM-SIC is still a problem. Then, GFDM-OQAM has been developed in [14]. However, GFDM-OQAM only keeps orthogonality in the real field so that it cannot be easily applied to the real channel. All approaches only aimed at eliminating the self-interference. And the interference in CE is still existing, which has been investigated in [15]–[21]. Two CE methods are proposed in [21]. In pilot-interference cancellation method, only the interference in pilot symbols is pre-canceled. This method needs to recalculate the interference value of pilot symbols each time, which increases the transmitter complexity. In transmitter interference cancellation method, the interference between data and pilot symbols is pre-canceled. However, the data vector needs to be pre-coded, which increases the correlation between data. Moreover, there are some problems when space-time block code (STBC) [22], [23] and space-frequency block code (SFBC) are applied to the GFDM system due to the non-orthogonal. In [24], [25], they propose two STBC schemes for GFDM system.

Manuscript received November 6, 2018; revised January 22, 2019; accepted February 25, 2019. Date of publication March 4, 2019; date of current version May 28, 2019. This work was supported by the National Nature Science Foundation of China under Grant 61671089. The review of this paper was coordinated by Prof. S.-H. Leung. This paper was presented in part at the IEEE Globecom Workshops, Washington, DC, USA, December 2016. *(Corresponding author: Kan Zheng.)*

F. Li, K. Zheng, L. Zhao, and H. Zhao are with the Beijing University of Posts and Telecommunications, Beijing 12472, China (e-mail: lifei870902@126.com; zkan@bupt.edu.cn; z-long@bupt.edu.cn; hzhao@bupt.edu.cn).

Y. Li is with the School of Electrical and Information Engineering, The University of Sydney, Sydney, NSW 2006, Australia (e-mail: yonghui.li@sydney.edu.au).

Digital Object Identifier 10.1109/TVT.2019.2902561

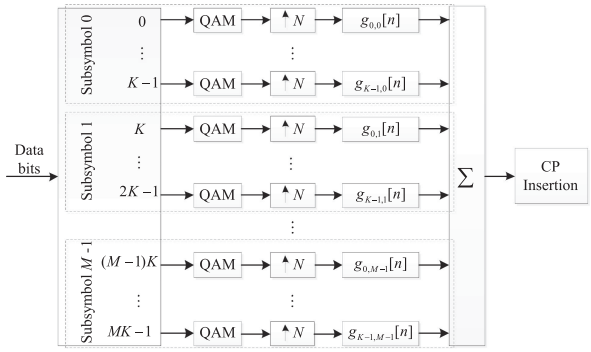

Fig. 1. The diagram of GFDM system.

However, the bit error rate (BER) performance is affected by the roll-off factor. Moreover, an even number of sub-symbols is required when combined with STBC. Therefore, it is necessary to set the first sub-symbol to zero. In brief, these existed researches bring in some disadvantages when reducing the impact on ICI, e.g., higher complexity, difficult to combine with channel estimation and performance loss caused by the roll-off factor. Thus, we propose a new GFDM transmission, i.e., GFDM-dual filter (GFDM-DF) in [1], which can transmit QAM symbols without intrinsic ICI on the assumption of ideal channel state information.

In this paper, we redesigned the filter from the frequency domain to further eliminate residual intrinsic interference. And GFDM-DF under the CE is also further developed. Then, how to apply it with MIMO technique is also discussed. Moreover, to verify the performances of the proposed GFDM-DF scheme, the signal to interference ratio (SIR) of GFDM-DF and conventional GFDM is analyzed. Besides, we design a low complexity receiver of GFDM-DF, which is suitable for the case where there are fewer sub-carriers and larger sub-symbols in a GFDM block. The GFDM-DF scheme uses two prototype filters on even-numbered and odd-numbered sub-carriers to address the problem caused by the self-interference. Therefore, an acceptable performance can be obtained by a simple linear receiver, e.g., matched filter (MF) receiver, which is not affected by the roll-off factor.

The rest of this paper is organized as follows. Section II introduces the GFDM system model. Then GFDM-DF scheme is proposed in Section III. Channel estimation for GFDM-DF scheme is presented in Section IV. Section V combines the GFDM-DF with SFBC and Section VI designs a low complexity GFDM-DF receiver. Section VII gives the numerical results. Finally, Section VIII concludes this paper.

II. System Model

Fig. 1 illustrates the diagram of GFDM system. The system first split the data bits into M sub-symbols and K sub-carriers [26], [27]. Then N point upsampling is applied to the data symbols, where $N = MK$. Each data symbol passing through their own filter $g[n]$, finally, the output signal without CP is given by

$$x[n] = \sum_{m=0}^{M-1} \sum_{k=0}^{K-1} d_{k,m} g_{k,m}[n],\ n = 0, \ldots, MK-1, \quad (1)$$

where

$$g_{k,m}[n] = g\left[(n - mK) \mod MK\right] \mathrm{e}^{-j2\pi \frac{kn}{K}}. \quad (2)$$

Equation (1) also can be seen as a matrix model

$$\mathbf{x} = \mathbf{A}\mathbf{d}, \quad (3)$$

$\mathbf{A}$ and $\mathbf{d}$ are expressed as follows

$$\mathbf{A} = \left[g_{0,0}[n] \ \cdots \ g_{K-1,0}[n]\ g_{0,1}[n] \ \cdots \ g_{K-1,M-1}[n]\right], \quad (4)$$

$$\mathbf{d} = \left[d_{0,0} \ \cdots \ d_{K-1,0}\ d_{0,1} \ \cdots \ d_{K-1,M-1}\right]^{\mathrm{T}}. \quad (5)$$

At the receiver side, the received signal after removing the CP is given by

$$\mathbf{y} = \mathbf{H}\mathbf{x} + \mathbf{n}, \quad (6)$$

where $\mathbf{n}$ is the AWGN. $\mathbf{H}$ is the circulant matrix of $\mathbf{h}$, and $\mathbf{h} = [h_0\ h_1\ \cdots\ h_{L-1}]$ is the channel time domain impulse response. Then the equalization can be easily applied in frequency domain as follows

$$\mathbf{y_e} = \mathcal{F}^{-1}\left\{\frac{\mathcal{F}(\mathbf{y})}{\mathcal{F}(\mathbf{h})}\right\}, \quad (7)$$

where $\mathcal{F}$ is the FFT, and $\mathcal{F}^{-1}$ is the inverse FFT (IFFT).

If a matched filter is applied to the receiver, and the noise is also ignored, the demodulation signal can be expressed as

$$\begin{aligned}\hat{d}_{k',m'} &= \sum_{n=-\infty}^{\infty} g^*_{k',m'}[n] \cdot y[n] \\ &= \sum_{n=-\infty}^{\infty} g^*_{k',m'}[n] \cdot \left\{\sum_{m=0}^{M-1}\sum_{k=0}^{K-1}\left(d_{k,m} g_{k,m}[n]\right)\right\} \\ &= d_{k',m'}\left\{\sum_{n=-\infty}^{\infty} g^*_{k',m'}[n] \cdot g_{k',m'}[n]\right\} \\ &\quad + \underbrace{\sum_{\substack{m\neq m'\\ k\neq k'}} d_{k,m}\left\{\sum_{n=-\infty}^{\infty} g^*_{k',m'}[n] \cdot g_{k,m}[n]\right\}}_{\text{interference from other symbols}}.\end{aligned} \quad (8)$$

As shown in equation (8), except the desired signal, it also introduces some interference from other symbols. Therefore, some linear receivers are introduced in [28].

1) MF Receiver:

$$\hat{\mathbf{d}} = \mathbf{A}^{\mathrm{H}} \cdot \mathbf{y_e}, \quad (9)$$

but the intrinsic self-interference cannot be removed by the MF receiver.

2) ZF Receiver:

$$\hat{\mathbf{d}} = \mathbf{A}^{+}\mathbf{y_e} \ \text{ with } \ \mathbf{A}^{+} = \left(\mathbf{A}^{\mathrm{H}}\mathbf{A}\right)^{-1}\mathbf{A}^{\mathrm{H}}, \quad (10)$$

the noise is amplified when using the ZF receiver.

3) MMSE Receiver:

$$\hat{\mathbf{d}} = \mathbf{A}^{\dagger}\mathbf{y_e} \ \text{ with } \ \mathbf{A}^{\dagger} = \left(\frac{\delta^2_{\mathbf{n}}}{\delta^2_{\mathbf{d}}}\mathbf{I} + \mathbf{A}^{\mathrm{H}}\mathbf{A}\right)^{-1}\mathbf{A}^{\mathrm{H}}, \quad (11)$$

although the performance of MMSE receiver is the best in three receivers, but the computational complexity is unpractical.

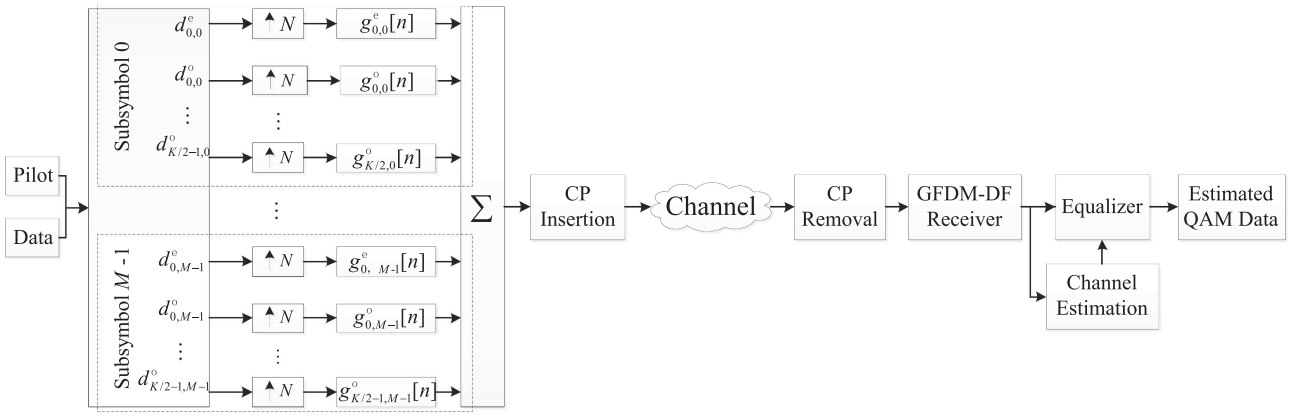

Fig. 2. The diagram of GFDM-DF scheme.

III. Proposed GFDM-DF Scheme Model

A GFDM-DF scheme model based on two filters was proposed, and the SIR of the GFDM-DF was evaluated in this section.

A. GFDM-DF Scheme

The scheme of GFDM-DF is shown in Fig. 2. In conventional GFDM, only one filter is used, here two different filters on the even-numbered and odd-numbered sub-carriers is used [29]. The information symbols $d_{k,m}$ are divided as follows

$$d^{\mathrm{e}}_{k,m} = d_{2k,m}\,, k \in \{0,\ 1,\ \ldots\ ,\ K/2-1\}\,, \tag{12}$$

$$d^{\mathrm{o}}_{k,m} = d_{2k+1,m}\,, k \in \{0,\ 1,\ \ldots\ ,\ K/2-1\}\,. \tag{13}$$

Then, the output signal can be obtained as follows

$$x[n] = \sum_{m=0}^{M-1}\sum_{k=0}^{K/2-1}\left(d^{\mathrm{e}}_{k,m}g^{\mathrm{e}}_{k,m}[n] + d^{\mathrm{o}}_{k,m}g^{\mathrm{o}}_{k,m}[n]\right), \tag{14}$$

where

$$g^{\mathrm{e}}_{k,m}[n] = g^{\mathrm{e}}\left[(n-mK)\mod MK\right]\mathrm{e}^{-j2\pi\frac{(2k)n}{K}}, \tag{15}$$

$$g^{\mathrm{o}}_{k,m}[n] = g^{\mathrm{o}}\left[(n-mK)\mod MK\right]\mathrm{e}^{-j2\pi\frac{(2k+1)n}{K}}, \tag{16}$$

g^{e} and g^{o} are two different filters which used on the even-numbered and odd-numbered sub-carriers, respectively.

At the receiver, the signal can be obtained after the MF receiver

$$\begin{aligned}\hat{d}^{\mathrm{e}}_{k',m'} &= \sum_{n=-\infty}^{\infty} g^{*\mathrm{e}}_{k',m'}[n]\cdot y[n]\\ &= \sum_{n=-\infty}^{\infty} g^{*\mathrm{e}}_{k',m'}[n]\cdot\left\{\sum_{m=0}^{M-1}\sum_{k=0}^{K/2-1}\begin{pmatrix} d^{\mathrm{e}}_{k,m}g^{\mathrm{e}}_{k,m}[n]\\ +d^{\mathrm{o}}_{k,m}g^{\mathrm{o}}_{k,m}[n]\end{pmatrix}\right\}\\ &= d^{\mathrm{e}}_{k',m'}\left\{\sum_{n=-\infty}^{\infty} g^{*\mathrm{e}}_{k',m'}[n]\cdot g^{\mathrm{e}}_{k',m'}[n]\right\}\\ &\quad+\underbrace{\sum_{\substack{m\neq m'\\ k\neq k'}} d^{\mathrm{e}}_{k,m}\left\{\sum_{n=-\infty}^{\infty} g^{*\mathrm{e}}_{k',m'}[n]\cdot g^{\mathrm{e}}_{k,m}[n]\right\}}_{\text{interference from other even-numbered symbols}}\\ &\quad+\underbrace{\sum_{m=0}^{M-1}\sum_{k=0}^{K/2-1} d^{\mathrm{o}}_{k,m}\left\{\sum_{n=-\infty}^{\infty} g^{*\mathrm{e}}_{k',m'}[n]\cdot g^{\mathrm{o}}_{k,m}[n]\right\}}_{\text{interference from odd-numbered symbols}},\end{aligned} \tag{17}$$

$$\begin{aligned}\hat{d}^{\mathrm{o}}_{k',m'} &= \sum_{n=-\infty}^{\infty} g^{*\mathrm{o}}_{k',m'}[n]\cdot y[n]\\ &= \sum_{n=-\infty}^{\infty} g^{*\mathrm{o}}_{k',m'}[n]\cdot\left\{\sum_{m=0}^{M-1}\sum_{k=0}^{K/2-1}\begin{pmatrix} d^{\mathrm{e}}_{k,m}g^{\mathrm{e}}_{k,m}[n]\\ +d^{\mathrm{o}}_{k,m}g^{\mathrm{o}}_{k,m}[n]\end{pmatrix}\right\}\\ &= d^{\mathrm{o}}_{k',m'}\left\{\sum_{n=-\infty}^{\infty} g^{*\mathrm{o}}_{k',m'}[n]\cdot g^{\mathrm{o}}_{k',m'}[n]\right\}\\ &\quad+\underbrace{\sum_{\substack{m\neq m'\\ k\neq k'}} d^{\mathrm{o}}_{k,m}\left\{\sum_{n=-\infty}^{\infty} g^{*\mathrm{o}}_{k',m'}[n]\cdot g^{\mathrm{o}}_{k,m}[n]\right\}}_{\text{interference from other odd-numbered symbols}}\\ &\quad+\underbrace{\sum_{m=0}^{M-1}\sum_{k=0}^{K/2-1} d^{\mathrm{e}}_{k,m}\left\{\sum_{n=-\infty}^{\infty} g^{*\mathrm{o}}_{k',m'}[n]\cdot g^{\mathrm{e}}_{k,m}[n]\right\}}_{\text{interference from even-numbered symbols}}\end{aligned} \tag{18}$$

As shown in equation (17), except the desired signal on even-numbered sub-carriers, there are also some interference from inter-symbol and odd-numbered symbols. Likewise, in equation (18), the signal also affected by the interference from inter-symbol and even-numbered symbols. To get the desired signal more accurately, the filter is best able to satisfy the orthogonality conditions as follows

$$condition\ 1\text{:}\quad \sum_{n=-\infty}^{\infty} g^{*\mathrm{e}}_{k',m'}[n]\cdot g^{\mathrm{e}}_{k,m}[n] = \delta_{k,k'}\delta_{m,m'}, \tag{19a}$$

$$condition\ 2:\ \sum_{n=-\infty}^{\infty} g^{*\mathrm{o}}_{k',m'}[n]\cdot g^{\mathrm{o}}_{k,m}[n]=\delta_{k,k'}\delta_{m,m'},\quad (19b)$$

$$condition\ 3:\ \sum_{n=-\infty}^{\infty} g^{*\mathrm{e}}_{k',m'}[n]\cdot g^{\mathrm{o}}_{k,m}[n]=0,.\quad (19c)$$

B. Matrix Model for the Proposed GFDM-DF Scheme

The matrix model of equation (14) can be expressed as

$$\mathbf{x}=\mathbf{A}^{\mathrm{e}}\mathbf{d}^{\mathrm{e}}+\mathbf{A}^{\mathrm{o}}\mathbf{d}^{\mathrm{o}},\quad (20)$$

where $\mathbf{A}^{\mathrm{e}}$ and $\mathbf{A}^{\mathrm{o}}$ only contain $g^{\mathrm{e}}_{k,m}[n]$ and $g^{\mathrm{o}}_{k,m}[n]$ respectively, which represented as

$$\mathbf{A}^{\mathrm{e}}=\left[g^{\mathrm{e}}_{0,0}[n]\ \cdots\ g^{\mathrm{e}}_{K/2-1,0}[n]\ \cdots\ g^{\mathrm{e}}_{K/2-1,M-1}[n]\right],\quad (21)$$

$$\mathbf{A}^{\mathrm{o}}=\left[g^{\mathrm{o}}_{0,0}[n]\ \cdots\ g^{\mathrm{o}}_{K/2-1,0}[n]\ \cdots\ g^{\mathrm{o}}_{K/2-1,M-1}[n]\right],\quad (22)$$

$\mathbf{d}^{\mathrm{e}}$ and $\mathbf{d}^{\mathrm{o}}$ are expressed as follows

$$\mathbf{d}^{\mathrm{e}}=\left[d^{\mathrm{e}}_{0,0}\ \cdots\ d^{\mathrm{e}}_{K/2-1,0}\ d^{\mathrm{e}}_{0,1}\ \cdots\ d^{\mathrm{e}}_{K/2-1,M-1}\right]^{\mathrm{T}},\quad (23)$$

$$\mathbf{d}^{\mathrm{o}}=\left[d^{\mathrm{o}}_{0,0}\cdots\ d^{\mathrm{o}}_{K/2-1,0}\ d^{\mathrm{o}}_{0,1}\ \cdots\ d^{\mathrm{o}}_{K/2-1,M-1}\right]^{\mathrm{T}}.\quad (24)$$

Therefore, equation (17) and (18) can be described as

$$\hat{\mathbf{d}}^{\mathrm{e}}=(\mathbf{A}^{\mathrm{e}})^{\mathrm{H}}\cdot\mathbf{x}=(\mathbf{A}^{\mathrm{e}})^{\mathrm{H}}\cdot\mathbf{A}^{\mathrm{e}}\mathbf{d}^{\mathrm{e}}+(\mathbf{A}^{\mathrm{e}})^{\mathrm{H}}\cdot\mathbf{A}^{\mathrm{o}}\mathbf{d}^{\mathrm{o}},\quad (25)$$

$$\hat{\mathbf{d}}^{\mathrm{o}}=(\mathbf{A}^{\mathrm{o}})^{\mathrm{H}}\cdot\mathbf{x}=(\mathbf{A}^{\mathrm{o}})^{\mathrm{H}}\cdot\mathbf{A}^{\mathrm{e}}\mathbf{d}^{\mathrm{e}}+(\mathbf{A}^{\mathrm{o}})^{\mathrm{H}}\cdot\mathbf{A}^{\mathrm{o}}\mathbf{d}^{\mathrm{o}}.\quad (26)$$

The orthogonality conditions in equation (19) are rewritten as

$$(\mathbf{A}^{\mathrm{e}})^{\mathrm{H}}\cdot\mathbf{A}^{\mathrm{e}}=\mathbf{I}_{MK/2},\quad (27a)$$

$$(\mathbf{A}^{\mathrm{o}})^{\mathrm{H}}\cdot\mathbf{A}^{\mathrm{o}}=\mathbf{I}_{MK/2},\quad (27b)$$

$$(\mathbf{A}^{\mathrm{e}})^{\mathrm{H}}\cdot\mathbf{A}^{\mathrm{o}}=\mathbf{0}_{MK/2}.\quad (27c)$$

C. The Filter Design

Equations (17) and (18) deduced the system interference model. Then, orthogonality conditions can be obtained from the interference model. Therefore, the appropriate filters need to be found out under the constraint of (19a)–(19c). The conventional GFDM uses the SRRC filter generated in the time domain, but here we generate the filter in the frequency domain according to the following equation

$$G(f)=\begin{cases}\sqrt{T}, & |f|\le\frac{1-\alpha}{2T}\\ \sqrt{\frac{T}{2}\left[1+\cos\left(\frac{\pi T}{\alpha}\left(|f|-\frac{1-\alpha}{2T}\right)\right)\right]}, & otherwise\cdot\\ 0, & |f|>\frac{1+\alpha}{2T}\end{cases}\quad (28)$$

The time domain filter $g[n]$ is then obtained by performing N-point IFFT on the frequency domain filter $G(f)$. We first treat $g[n]$ as g^{e}. Then, g^{o} can be obtained by the following rule [30]

$$g^{\mathrm{o}}=\left[g^{(2M-1)}\ g^{(2M-2)}\ g^{(2M-3)}\ g^{(2M-4)}\ \cdots\ g^{(0)}\right],\quad (29)$$

where $g^{(l)}\ (l=0,1,\ldots,2M-1)$ is derived from the g^{e} as follows

$$g^{\mathrm{e}}=\left[g^{(0)}\ g^{(1)}\ g^{(2)}\ g^{(3)}\ \cdots\ g^{(2M-1)}\right],\quad (30)$$

and the length of $g^{(l)}$ is $K/2$ [1].

Fig. 3 shows the response of $\mathbf{A}^{\mathrm{H}}\cdot\mathbf{A}$, $(\mathbf{A}^{\mathrm{e}})^{\mathrm{H}}\cdot\mathbf{A}^{\mathrm{e}}$ and $(\mathbf{A}^{\mathrm{o}})^{\mathrm{H}}\cdot\mathbf{A}^{\mathrm{e}}$ in dB [31]. In Fig. 3(a), it is obvious to observe that the intrinsic self-interference on the secondary diagonals, which is the self-interference between adjacent sub-carriers. However, in Fig. 3(c), the intrinsic self-interference on the secondary diagonals is handled. Fig. 3(c) also shows that the self-interference between odd-numbered and even-numbered sub-carriers barely exist, and it can be ignored.

D. Signal-to-Interference Ratio Evaluation

In this part, the SIR for GFDM-DF and conventional GFDM is evaluated. The selected filter in conventional GFDM is SRRC, g^{e} and g^{o} are used for GFDM-DF. According to equation (17), the SIR on even-numbered sub-carriers is given by equation (31) shown at the bottom of this page. Similarly, equation (32) shown at the bottom of this page, also gives the SIR on odd-numbered sub-carriers [32].

Table I shows the SIR of the GFDM-DF and conventional GFDM. The SIR value of GFDM-DF is much larger than GFDM. Moreover, with the roll-off factor α increases, the SIR of conventional GFDM becomes small, However, the SIR of GFDM-DF

$$SIR^{\mathrm{e}}=\frac{E\left[\left|d^{\mathrm{e}}_{k,m}\right|^2\right]\cdot\left\{\left|\sum_{n=-\infty}^{\infty}g^{*\mathrm{e}}_{k',m'}[n]\cdot g^{\mathrm{e}}_{k',m'}[n]\right|^2\right\}}{E\left[\left|d^{\mathrm{e}}_{k,m}\right|^2\right]\cdot\sum_{\substack{m\neq m'\\k\neq k'}}\left\{\left|\sum_{n=-\infty}^{\infty}g^{*\mathrm{e}}_{k',m'}[n]\cdot g^{\mathrm{e}}_{k,m}[n]\right|^2\right\}+E\left[\left|d^{\mathrm{o}}_{k,m}\right|^2\right]\cdot\sum_{m=0}^{M-1}\sum_{k=0}^{K/2-1}\left\{\left|\sum_{n=-\infty}^{\infty}g^{*\mathrm{e}}_{k',m'}[n]\cdot g^{\mathrm{o}}_{k,m}[n]\right|^2\right\}}.\quad (31)$$

$$SIR^{\mathrm{o}}=\frac{E\left[\left|d^{\mathrm{o}}_{k,m}\right|^2\right]\cdot\left\{\left|\sum_{n=-\infty}^{\infty}g^{*\mathrm{o}}_{k',m'}[n]\cdot g^{\mathrm{o}}_{k',m'}[n]\right|^2\right\}}{E\left[\left|d^{\mathrm{o}}_{k,m}\right|^2\right]\cdot\sum_{\substack{m\neq m'\\k\neq k'}}\left\{\left|\sum_{n=-\infty}^{\infty}g^{*\mathrm{o}}_{k',m'}[n]\cdot g^{\mathrm{o}}_{k,m}[n]\right|^2\right\}+E\left[\left|d^{\mathrm{e}}_{k,m}\right|^2\right]\cdot\sum_{m=0}^{M-1}\sum_{k=0}^{K/2-1}\left\{\left|\sum_{n=-\infty}^{\infty}g^{*\mathrm{o}}_{k',m'}[n]\cdot g^{\mathrm{e}}_{k,m}[n]\right|^2\right\}}.\quad (32)$$

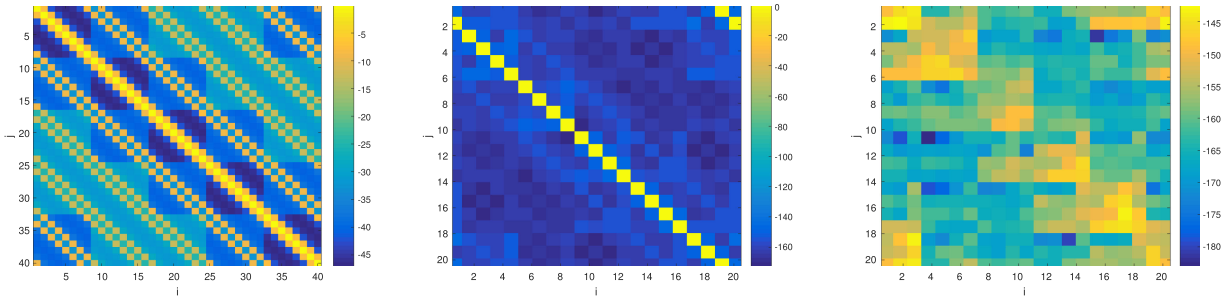

(a) $\mathbf{A}^{\mathrm{H}} \cdot \mathbf{A}$ (b) $(\mathbf{A}^{\mathrm{e}})^{\mathrm{H}} \cdot \mathbf{A}^{\mathrm{e}}$ (c) $(\mathbf{A}^{\mathrm{o}})^{\mathrm{H}} \cdot \mathbf{A}^{\mathrm{e}}$

Fig. 3. Crosstalk response of the matched filter receiver without noise. Each tile denotes the amplitude of $\left[\mathbf{A}^{\mathrm{H}} \cdot \mathbf{A}\right]_{ij}$, $[(\mathbf{A}^{\mathrm{e}})^{\mathrm{H}} \cdot \mathbf{A}^{\mathrm{e}}]_{i,j}$, and $[(\mathbf{A}^{\mathrm{o}})^{\mathrm{H}} \cdot \mathbf{A}^{\mathrm{e}}]_{i,j}$ in dB. A SRRC filter is used with $\alpha = 0.5$ and $M = 5$, and $K = 8$.

TABLE I
THE SIR OF GFDM AND GFDM-DF

	GFDM SIR	GFDM-DF SIR	
α=0.1	18.8 dB	Even-numbered sub-carriers	260.8 dB
		Odd-numbered sub-carriers	259.1 dB
α=0.9	6.5 dB	Even-numbered sub-carriers	260.5 dB
		Odd-numbered sub-carriers	258.6 dB

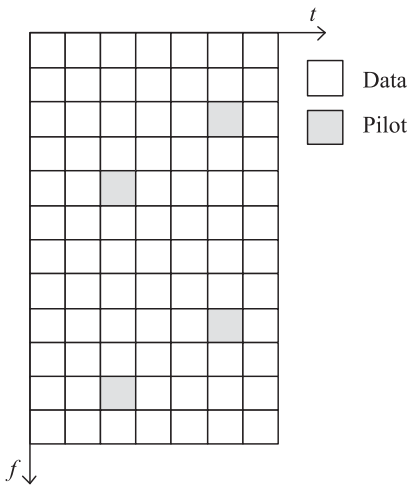

Fig. 4. Pilot positions of per RB in seven symbols.

is about 260 dB no matter how the roll-off factor changes. Although GFDM suffers from the ICI and ISI simultaneously, ICI is the main interference. When α increases, the ICI between adjacent carriers becomes large. But in the proposed GFDM-DF, there is no ICI and ISI, hence, no matter how α changes, it does not have any effect on SIR.

IV. CHANNEL ESTIMATION FOR GFDM-DF SCHEME

Our purpose is to verify whether GFDM and GFDM-DF scheme can use the same CE method used in OFDM system. Therefore, we choose the same least squares (LS) CE method used in OFDM, GFDM and GFDM-DF. Fig. 4 describes the pilot positions in seven symbols with two symbols selected in each RB, and two pilots for each symbol.

At the receiver side, the received signal after removing the CP is given by

$$\mathbf{y} = \mathbf{H}\mathbf{x} + \mathbf{n}, \tag{33}$$

where $\mathbf{x} = \mathbf{A}^{\mathrm{e}}\mathbf{d}^{\mathrm{e}} + \mathbf{A}^{\mathrm{o}}\mathbf{d}^{\mathrm{o}}$ and $\mathbf{H}$ is the circulant matrix of the channel. After GFDM-DF detector, the demodulation signal can be expressed as

$$\hat{\mathbf{d}}^{\mathrm{e}} = (\mathbf{A}^{\mathrm{e}})^{\mathrm{H}} \cdot \mathbf{y} = \bar{H}^{\mathrm{e}}\mathbf{d}^{\mathrm{e}} + W^{\mathrm{e}}, \tag{34}$$

$$\hat{\mathbf{d}}^{\mathrm{o}} = (\mathbf{A}^{\mathrm{o}})^{\mathrm{H}} \cdot \mathbf{y} = \bar{H}^{\mathrm{o}}\mathbf{d}^{\mathrm{o}} + W^{\mathrm{o}}, \tag{35}$$

where $\bar{H}^{\mathrm{e}}$ and $\bar{H}^{\mathrm{o}}$ denote effective channel in frequency domain on the even-numbered and odd-numbered sub-carriers, respectively. W^{e} and W^{o} are the noise in frequency domain on even-numbered and odd-numbered sub-carriers, respectively. Then, combine equation (34) and (35), the demodulation signal is presented as

$$\hat{\mathbf{d}} = \bar{H}\mathbf{d} + W, \tag{36}$$

The channel coefficient $\bar{H}$ denotes the FFT transformed effective channel, consisting of the transmitter filter, the receiver filter and the mobile channel [9]

$$\bar{H}[n] = \mathcal{F}\left\{g_{Tx}[n] * g_{Rx}[n] * h[n]\right\}. \tag{37}$$

Thus, the equalization needs to be done after the MF, ZF or MMSE detector.

The normalized value of the LS method can be expressed as

$$\bar{H}_{LS} = \arg\min\left\{\left(\hat{\mathbf{d}} - \bar{H}\mathbf{d}\right)^{H}\left(\hat{\mathbf{d}} - \bar{H}\mathbf{d}\right)\right\}. \tag{38}$$

We can obtain the approximate channel coefficient using LS estimation at pilot position after the detector as below

$$\bar{H}_{LS_p} = \frac{\hat{\mathbf{d}}_p}{\mathbf{d}_p}, \tag{39}$$

where $\hat{\mathbf{d}}_p$ and $\mathbf{d}_p$ denote the pilot position in $\hat{\mathbf{d}}$ and $\mathbf{d}$, respectively. After interpolation method, we can obtain the whole channel characteristics $\bar{H}_{LS}$ [33].

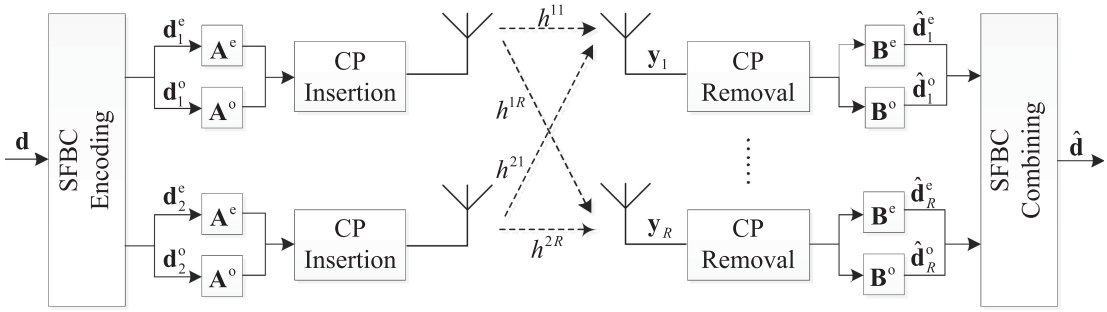

Fig. 5. The diagram of MIMO GFDM-DF system with SFBC.

V. Space-Frequency Block Coding for GFDM-DF Scheme

One of the most important goals of next generation cellular systems is to achieve high throughput communication, the SFBC proposed by Alamouti provides a simple method to achieve transmit diversity [34]. Since OFDM is an orthogonal system, it is easy to combine with Alamouti-SFBC. However, for GFDM, the sub-symbols in each GFDM block are superimposed, and there also has large interference between adjacent sub-carriers. Therefore, the directly combined with Alamouti-SFBC in one GFDM block is problematical. The major contribution of this section is to introduce a feasible scheme which applies SFBC to GFDM-DF scheme. The simplified diagram for a MIMO GFDM-DF scheme with SFBC is shown in Fig. 5.

The transmit data $\mathbf{d}$ from equation (5) is first applied to the SFBC encoding, and the output signal of SFBC $\mathbf{d}_1$ and $\mathbf{d}_2$ are defined as follows

$$\mathbf{d}_1 = \begin{bmatrix} d_{0,0} & -d_{1,0}^* & \cdots & d_{K-2,0} & -d_{K-1,0}^* \\ & \cdots & d_{K-2,M-1} & -d_{K-1,M-1}^* & \end{bmatrix}^{\mathrm{T}}, \tag{40}$$

$$\mathbf{d}_2 = \begin{bmatrix} d_{1,0} & d_{0,0}^* & \cdots & d_{K-1,0} & d_{K-2,0}^* \\ & \cdots & d_{K-1,M-1} & d_{K-2,M-1}^* & \end{bmatrix}^{\mathrm{T}}. \tag{41}$$

Then the data symbols $\mathbf{d}_1$ and $\mathbf{d}_2$ are divided into $\mathbf{d}_1^{\mathrm{e}}$, $\mathbf{d}_2^{\mathrm{e}}$ and $\mathbf{d}_1^{\mathrm{o}}$, $\mathbf{d}_2^{\mathrm{o}}$, respectively,

$$\mathbf{d}_1^{\mathrm{e}} = [d_{0,0} \ \cdots \ d_{K-2,0} \ \cdots \ d_{K-2,M-1}]^{\mathrm{T}}, \tag{42}$$

$$\mathbf{d}_2^{\mathrm{e}} = [d_{1,0} \ \cdots \ d_{K-1,0} \ \cdots \ d_{K-1,M-1}]^{\mathrm{T}}, \tag{43}$$

$$\mathbf{d}_1^{\mathrm{o}} = [-d_{1,0}^* \ \cdots \ -d_{K-1,0}^* \ \cdots \ -d_{K-1,M-1}^*]^{\mathrm{T}}, \tag{44}$$

$$\mathbf{d}_2^{\mathrm{o}} = [d_{0,0}^* \ \cdots \ d_{K-2,0}^* \ \cdots \ d_{K-2,M-1}^*]^{\mathrm{T}}. \tag{45}$$

The data $\mathbf{d}_1^{\mathrm{e}}$, $\mathbf{d}_2^{\mathrm{e}}$, $\mathbf{d}_1^{\mathrm{o}}$ and $\mathbf{d}_2^{\mathrm{o}}$ are independently modulated with the GFDM-DF transmitter matrices $\mathbf{A}^{\mathrm{e}}$ and $\mathbf{A}^{\mathrm{o}}$. After CP removed, the receive signal $\mathbf{y}^r$ at receive antenna r is written as

$$\mathbf{y}^r = \mathbf{H}^{1r}(\mathbf{A}^{\mathrm{e}}\mathbf{d}_1^{\mathrm{e}} + \mathbf{A}^{\mathrm{o}}\mathbf{d}_1^{\mathrm{o}}) + \mathbf{H}^{2r}(\mathbf{A}^{\mathrm{e}}\mathbf{d}_2^{\mathrm{e}} + \mathbf{A}^{\mathrm{o}}\mathbf{d}_2^{\mathrm{o}}) + \mathbf{n}_r, \tag{46}$$

where $\mathbf{H}^{tr}$ is the circulant channel matrix and the first line of $\mathbf{H}^{tr}$ is the multi-path channel impulse response (CIR) h^{tr}.

On the receiver side, before SFBC combination, the signal on each receive antenna is demodulated by $\mathbf{B}^{\mathrm{e}}$ and $\mathbf{B}^{\mathrm{o}}$, respectively,

$$\hat{\mathbf{d}}_r^{\mathrm{e}} = \mathbf{B}^{\mathrm{e}} \cdot \mathbf{y}^r = H^{1r}\mathbf{d}_1^{\mathrm{e}} + H^{2r}\mathbf{d}_2^{\mathrm{e}} + \bar{\mathbf{n}}_r^{\mathrm{e}}, \tag{47}$$

$$\hat{\mathbf{d}}_r^{\mathrm{o}} = \mathbf{B}^{\mathrm{o}} \cdot \mathbf{y}^r = H^{1r}\mathbf{d}_1^{\mathrm{o}} + H^{2r}\mathbf{d}_2^{\mathrm{o}} + \bar{\mathbf{n}}_r^{\mathrm{o}}, \tag{48}$$

where $\mathbf{B}^{\mathrm{e}}$ and $\mathbf{B}^{\mathrm{o}}$ are the receiver matrices, and they can be the MF, ZF or MMSE matrix, but here we just regard $\mathbf{B}^{\mathrm{e}} = (\mathbf{A}^{\mathrm{e}})^{\mathrm{H}}$ and $\mathbf{B}^{\mathrm{o}} = (\mathbf{A}^{\mathrm{o}})^{\mathrm{H}}$ as the MF receiver matrices. H^{tr} means the FFT of the CIR h^{tr}.

Then we combine the data in equation (47) and (48) to obtain

$$\hat{\mathbf{d}}_r = H^{1r}\mathbf{d}_1 + H^{2r}\mathbf{d}_2 + \bar{\mathbf{n}}_r. \tag{49}$$

We can also describe equation (49) in detail as follows

$$\hat{d}_{k,m}^r = H_{k,m}^{1r} d_{k,m} + H_{k,m}^{2r} d_{k+1,m} + \bar{n}_{k,m}^r, \tag{50}$$

$$\hat{d}_{k+1,m}^r = H_{k+1,m}^{1r}(-d_{k+1,m}^*) + H_{k+1,m}^{2r} d_{k,m}^* + \bar{n}_{k+1,m}^r, \tag{51}$$

where $H_{k,m}^{tr}$ and $\hat{d}_{k,m}^r$ denote the kth sub-carrier and mth sub-symbol of H^{tr} and $\hat{\mathbf{d}}^r$ on the receive antenna r, respectively. Then, the SFBC combining is carried out separately

$$d_{k,m} = \frac{\sum_{r=1}^{R} (H_{k,m}^{1r})^* \hat{d}_{k,m}^r + H_{k,m}^{2r} (\hat{d}_{k+1,m}^r)^*}{\sum_{r=1}^{R} \left|H_{k,m}^{1r}\right|^2 + \left|H_{k,m}^{2r}\right|^2} + \tilde{n}_{k,m}, \tag{52}$$

$$d_{k+1,m} = \frac{\sum_{r=1}^{R} (H_{k,m}^{2r})^* \hat{d}_{k,m}^r - H_{k,m}^{1r} (\hat{d}_{k+1,m}^r)^*}{\sum_{r=1}^{R} \left|H_{k,m}^{1r}\right|^2 + \left|H_{k,m}^{2r}\right|^2} + \tilde{n}_{k+1,m}. \tag{53}$$

VI. Low Complexity GFDM-DF Scheme Receiver Design

Since GFDM-DF uses matrices to receive the signal, which brings large number of matrix operations. In this section, we consider low complexity receiver for GFDM-DF scheme [35], [36].

Without any loss of generality, the signal at the receiver is expressed as

$$\mathbf{y} = \mathbf{A}^{\mathrm{e}}\mathbf{d}^{\mathrm{e}} + \mathbf{A}^{\mathrm{o}}\mathbf{d}^{\mathrm{o}} + \mathbf{n}. \tag{54}$$

First, we apply a MK point FFT on both sides of equation (54), and according to $\mathcal{F}_{MK/2}^{-1}\mathcal{F}_{MK/2} = \mathbf{I}$, the above equation can be expressed as

$$\mathcal{F}_{MK}\mathbf{y} = \mathcal{F}_{MK}\mathbf{A}^{\mathrm{e}}\mathcal{F}_{MK/2}^{-1}\mathcal{F}_{MK/2}\mathbf{d}^{\mathrm{e}} + \mathcal{F}_{MK}\mathbf{A}^{\mathrm{o}}\mathcal{F}_{MK/2}^{-1}F_{MK/2}\mathbf{d}^{\mathrm{o}} + \mathcal{F}_{MK}\mathbf{n}. \tag{55}$$

Let $\mathbf{B}^{\mathrm{e}} = \mathcal{F}_{MK}\mathbf{A}^{\mathrm{e}}\mathcal{F}^{-1}_{MK/2}$ and $\mathbf{B}^{\mathrm{o}} = \mathcal{F}_{MK}\mathbf{A}^{\mathrm{o}}\mathcal{F}^{-1}_{MK/2}$, where $\mathbf{B}^{\mathrm{e}} = [\mathbf{B}^{\mathrm{e}(1)}\mathbf{B}^{\mathrm{e}(2)}\cdots\mathbf{B}^{\mathrm{e}(K/2)}]$ and $\mathbf{B}^{\mathrm{o}} = [\mathbf{B}^{\mathrm{o}(1)}\mathbf{B}^{\mathrm{o}(2)}\cdots\mathbf{B}^{\mathrm{o}(K/2)}]$. Then equation (55) can be rewritten as

$$\bar{\mathbf{y}} = \mathbf{B}^{\mathrm{e}}\bar{\mathbf{d}}^{\mathrm{e}} + \mathbf{B}^{\mathrm{o}}\bar{\mathbf{d}}^{\mathrm{o}} + \bar{\mathbf{n}}, \tag{56}$$

where $\bar{\mathbf{y}}$, $\bar{\mathbf{d}}$ and $\bar{\mathbf{n}}$ denote the frequency signal of $\mathbf{y}$, $\mathbf{d}$ and $\mathbf{n}$, respectively.

We investigate the structure of $\mathbf{B}^{\mathrm{e}}$ and $\mathbf{B}^{\mathrm{o}}$, and we found that $\mathbf{B}^{\mathrm{e}(k)}$ has the following characteristic

$$\mathbf{B}^{\mathrm{e}(k)} = \begin{bmatrix} b_1^{\mathrm{e}(k)} & 0 & \cdots & 0 \\ 0 & b_2^{\mathrm{e}(k)} & \cdots & 0 \\ \vdots & \vdots & \ddots & \vdots \\ 0 & 0 & \cdots & b_M^{\mathrm{e}(k)} \\ b_{M+1}^{\mathrm{e}(k)} & 0 & \cdots & 0 \\ 0 & b_{M+2}^{\mathrm{e}(k)} & \cdots & 0 \\ \vdots & \vdots & \ddots & \vdots \\ 0 & 0 & \cdots & b_{2M}^{\mathrm{e}(k)} \\ \ddots & & & \\ & \ddots & & \\ & & \ddots & \\ & & & \ddots \\ b_{(K-1)M+1}^{\mathrm{e}(k)} & 0 & \cdots & 0 \\ 0 & b_{(K-1)M+2}^{\mathrm{e}(k)} & \cdots & 0 \\ \vdots & \vdots & \ddots & \vdots \\ 0 & 0 & \cdots & b_{KM}^{\mathrm{e}(k)} \end{bmatrix}, \tag{57}$$

where $k = 1, 2, \cdots, K/2$, and $\mathbf{B}^{\mathrm{o}(k)}$ also has the same characteristic. We can rearrange $\mathbf{B}^{\mathrm{e}}$ and $\mathbf{B}^{\mathrm{o}}$ into block diagonal matrices through row and column permutation by selecting one in every M rows and selecting one in every M columns, then pile them together. Matrices $\mathbf{B}^{\mathrm{e}}$ and $\mathbf{B}^{\mathrm{o}}$ can be reorganized into block diagonal matrices $\tilde{\mathbf{B}}^{\mathrm{e}}$ and $\tilde{\mathbf{B}}^{\mathrm{o}}$ by row and column permutations as shown in equation (58) at the bottom of this page. Then, $\tilde{\mathbf{B}}^{\mathrm{e}}$ and $\tilde{\mathbf{B}}^{\mathrm{o}}$ can be rewritten as

$$\tilde{\mathbf{B}}^{\mathrm{e}} = \begin{bmatrix} \tilde{\mathbf{B}}_1^{\mathrm{e}} & & & \\ & \tilde{\mathbf{B}}_2^{\mathrm{e}} & & \\ & & \ddots & \\ & & & \tilde{\mathbf{B}}_M^{\mathrm{e}} \end{bmatrix}_{MK\times MK/2}, \tag{59}$$

$$\tilde{\mathbf{B}}^{\mathrm{o}} = \begin{bmatrix} \tilde{\mathbf{B}}_1^{\mathrm{o}} & & & \\ & \tilde{\mathbf{B}}_2^{\mathrm{o}} & & \\ & & \ddots & \\ & & & \tilde{\mathbf{B}}_M^{\mathrm{o}} \end{bmatrix}_{MK\times MK/2}, \tag{60}$$

where $\tilde{\mathbf{B}}_m^{\mathrm{e}}$ and $\tilde{\mathbf{B}}_m^{\mathrm{o}}$ are $K \times K/2$ matrices. And the structure of $\tilde{\mathbf{B}}_m^{\mathrm{e}}$ is represented as

$$\tilde{\mathbf{B}}_m^{\mathrm{e}} = \begin{bmatrix} b_m^{\mathrm{e}(1)} & b_m^{\mathrm{e}(2)} & \cdots & b_m^{\mathrm{e}(K/2)} \\ b_{M+m}^{\mathrm{e}(1)} & b_{M+m}^{\mathrm{e}(2)} & \cdots & b_{M+m}^{\mathrm{e}(K/2)} \\ \vdots & \vdots & \ddots & \vdots \\ b_{(K-1)M+m}^{\mathrm{e}(1)} & b_{(K-1)M+m}^{\mathrm{e}(2)} & \cdots & b_{(K-1)M+m}^{\mathrm{e}(K/2)} \end{bmatrix}, \tag{61}$$

To ensure equality on both sides of the equation, $\bar{\mathbf{y}}$ and $\bar{\mathbf{n}}$ also perform the same row arrangement as $\mathbf{B}^{\mathrm{e}}$ and $\mathbf{B}^{\mathrm{o}}$ to get $\tilde{\mathbf{y}}$ and $\tilde{\mathbf{n}}$. $\bar{\mathbf{d}}$ also performs the same column arrangement as $\mathbf{B}^{\mathrm{e}}$ and $\mathbf{B}^{\mathrm{o}}$ to get $\tilde{\mathbf{d}}$. Thus, the arranged expression can be written as

$$\tilde{\mathbf{y}} = \tilde{\mathbf{B}}^{\mathrm{e}}\tilde{\mathbf{d}}^{\mathrm{e}} + \tilde{\mathbf{B}}^{\mathrm{o}}\tilde{\mathbf{d}}^{\mathrm{o}} + \tilde{\mathbf{n}}. \tag{62}$$

Since $\tilde{\mathbf{B}}^{\mathrm{e}}$ and $\tilde{\mathbf{B}}^{\mathrm{o}}$ are block diagonal matrices, equation (62) can be reordered into M equation sets

$$\tilde{\mathbf{y}}_m = \tilde{\mathbf{B}}_m^{\mathrm{e}}\tilde{\mathbf{d}}_m^{\mathrm{e}} + \tilde{\mathbf{B}}_m^{\mathrm{o}}\tilde{\mathbf{d}}_m^{\mathrm{o}} + \tilde{\mathbf{n}}_m. \tag{63}$$

$$\tilde{\mathbf{B}}^{\mathrm{e}} = \begin{bmatrix} b_1^{\mathrm{e}(1)} & b_1^{\mathrm{e}(2)} & \cdots & b_1^{\mathrm{e}(K/2)} & 0 & 0 & 0 & 0 & \\ b_{M+1}^{\mathrm{e}(1)} & b_{M+1}^{\mathrm{e}(2)} & \cdots & b_{M+1}^{\mathrm{e}(K/2)} & 0 & 0 & 0 & 0 & \\ \vdots & \vdots & \ddots & \vdots & \vdots & \vdots & \ddots & \vdots & \\ b_{(K-1)M+1}^{\mathrm{e}(1)} & b_{(K-1)M+1}^{\mathrm{e}(2)} & \cdots & b_{(K-1)M+1}^{\mathrm{e}(K/2)} & 0 & 0 & \cdots & 0 & \\ 0 & 0 & \cdots & 0 & b_2^{\mathrm{e}(1)} & b_2^{\mathrm{e}(2)} & \cdots & b_2^{\mathrm{e}(K/2)} & \cdots \\ 0 & 0 & \cdots & 0 & b_{M+2}^{\mathrm{e}(1)} & b_{M+2}^{\mathrm{e}(2)} & \cdots & b_{M+2}^{\mathrm{e}(K/2)} & \\ \vdots & \vdots & \ddots & \vdots & \vdots & \vdots & \ddots & \vdots & \\ 0 & 0 & & 0 & b_{(K-1)M+2}^{\mathrm{e}(1)} & b_{(K-1)M+2}^{\mathrm{e}(2)} & \cdots & b_{(K-1)M+2}^{\mathrm{e}(K/2)} & \\ & & & \vdots & & & & & \ddots \end{bmatrix} \tag{58}$$

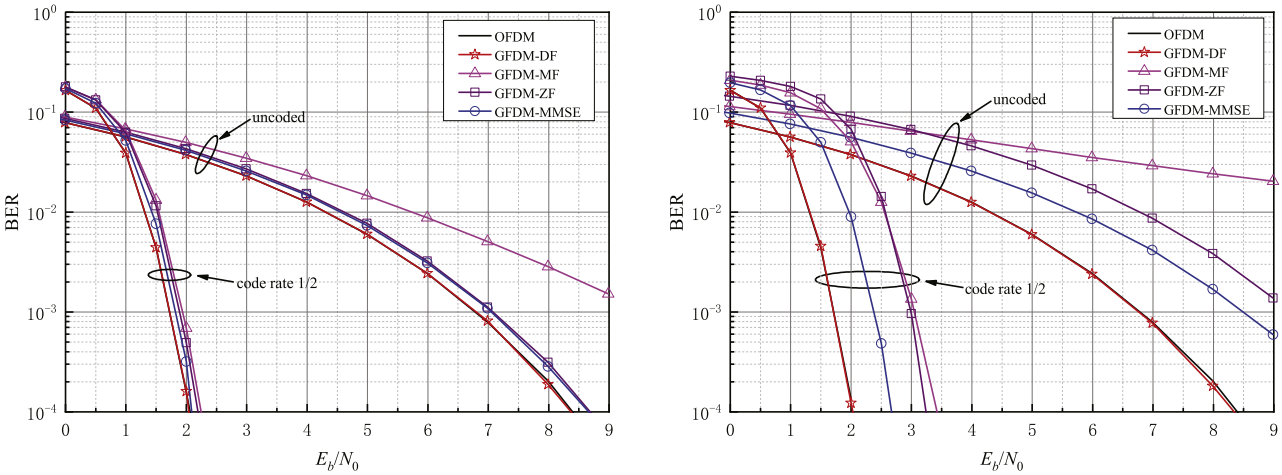

(a) $M = 7, K = 128$, and $\alpha = 0.25$ (b) $M = 7, K = 128$, and $\alpha = 0.75$

Fig. 6. BER performance comparison in AWGN channel with Turbo code rate 1/2. (a) $M = 7, K = 128$, and $\alpha = 0.25$. (b) $M = 7, K = 128$, and $\alpha = 0.75$.

TABLE II
SIMULATION PARAMETERS FOR THE PROPOSED GFDM-DF SCHEME

Parameter	Value	
	OFDM	GFDM/GFDM-DF
Modulation	QPSK, 64QAM	
Samples per symbol K	128	128
Active sub-carriers K_{on}	36	36
Block size (symbols) M	7	7
Subcarrier spacing (kHz)	15	15
CP length (samples) N_{CP}	32	32
Filter	Rectangular	SRRC
Roll-off factor α	-	0.25, 0.75
Channel model $h[n]$	AWGN, EPA, Rayleigh	
EPA delay (ns)	[0 30 70 90 110 190 410]	
EPA power (dB)	[0.0 -1.0 -2.0 -3.0 -8.0 -17.2 -20.8]	
Rayleigh delay (ns)	[0 30 150 260 370 710 1090]	
Rayleigh power (dB)	[0.0 -1.5 -4.9 -16.9 -17.2 -20.8 -23.9]	
Channel coding	Turbo code [37] 5 iterations	
Pilot spacing (subcarriers)	6	
Estimation algorithm	LS	

According to equation (63), the demodulation signal $\tilde{\mathbf{d}}_m^{\mathrm{e}'}$ and $\tilde{\mathbf{d}}_m^{\mathrm{o}'}$ can be obtained as follows

$$\tilde{\mathbf{d}}_m^{\mathrm{e}'} = (\tilde{\mathbf{B}}_m^{\mathrm{e}})^{\mathrm{H}} \cdot \tilde{\mathbf{y}}_m, \tag{64}$$

$$\tilde{\mathbf{d}}_m^{\mathrm{o}'} = (\tilde{\mathbf{B}}_m^{\mathrm{o}})^{\mathrm{H}} \cdot \tilde{\mathbf{y}}_m. \tag{65}$$

We need to select one in every M columns of $\tilde{\mathbf{d}}^{\mathrm{e}'}$ and $\tilde{\mathbf{d}}^{\mathrm{o}'}$ and pile them together to get $\bar{\mathbf{d}}^{\mathrm{e}'}$ and $\bar{\mathbf{d}}^{\mathrm{o}'}$, then perform $MK/2$ point IFFT to get $\mathbf{d}^{\mathrm{e}'}$ and $\mathbf{d}^{\mathrm{o}'}$. After combining $\mathbf{d}^{\mathrm{e}'}$ and $\mathbf{d}^{\mathrm{o}'}$, we can obtain the final signal $\mathbf{d}'$.

VII. NUMERICAL RESULTS

In this section, the performance of GFDM-DF scheme is evaluated, and Table II shows the detailed simulation parameters.

A. Performance Comparison in AWGN Channel

As shown in Fig. 6, in case of low SNR region, the noise is dominant and all the performance of the three receivers in the conventional GFDM system is close to the OFDM system. But at high SNR region, the noise power decreases and the intrinsic self-interference becomes the main effect factor, the BER of MF receiver deviates from the others. As the roll-off factor α increases, the performance of conventional GFDM deviates from the OFDM system seriously. However, the GFDM-DF can always maintain the same BER performance as OFDM system.

The Turbo coded BER performance is also evaluated in Fig. 6. The proposed GFDM-DF can achieve the same performance compared with OFDM no matter how the roll-off factor α changes. However, the performance of conventional GFDM becomes worse as the roll-off factor α increases.

B. Performance Comparison in Multi-Path Channel

1) EPA Channel: The BER performance of the various scheme is shown in Fig. 7 with LS CE in Extended Pedestrian A (EPA) channel. It can be seen from Fig. 7(a) that both GFDM-DF and conventional GFDM can achieve the same performance as OFDM in the low SNR region. But in Fig. 7(b), when $\alpha = 0.75$, the BER performance of conventional GFDM system deviates from the OFDM system. Particularly, the performance of MF receiver becomes worse due to the intrinsic self-interference. This also explains that the performance of conventional GFDM system relies heavily on the choice of roll-off factor α. However, GFDM-DF can achieve the same performance as OFDM in the low SNR region. On the other hand, in the high SNR region, the performance of GFDM-DF is worse than OFDM duo to the effects of ISI. We also evaluated the coding performance in multi-path channels, the code word length after the rate matching is 480 and the detailed coding type is given as ones in LTE [37]. It can be seen from the coded performance that the curve of GFDM-DF is consistent with OFDM. However, the coding performance of conventional GFDM becomes worse than OFDM with the increase of α.

2) Rayleigh Fading Channel: Compared to Fig. 7, the BER performance in Rayleigh fading channel is similar to that of EPA channel. However, the effect of ISI becomes larger, which results in a slight decrease in BER performance. Moreover, there is an obvious decrease in BER performance of GFDM-DF with

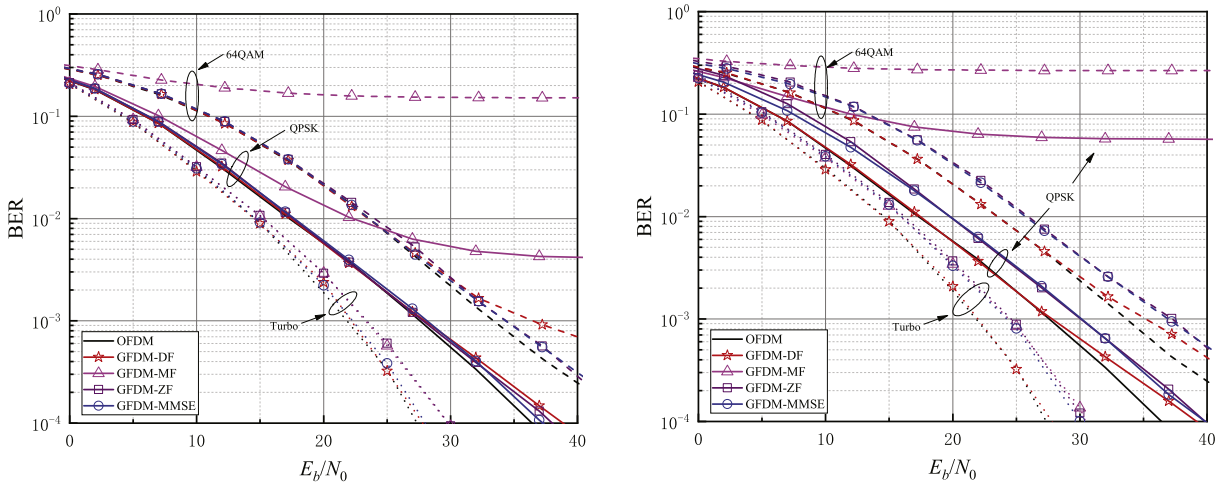

(a) $M = 7, K = 128$, and $\alpha = 0.25$ (b) $M = 7, K = 128$, and $\alpha = 0.75$

Fig. 7. BER performance comparison in EPA channel with LS channel estimation. (a) $M = 7, K = 128$, and $\alpha = 0.25$. (b) $M = 7, K = 128$, and $\alpha = 0.75$.

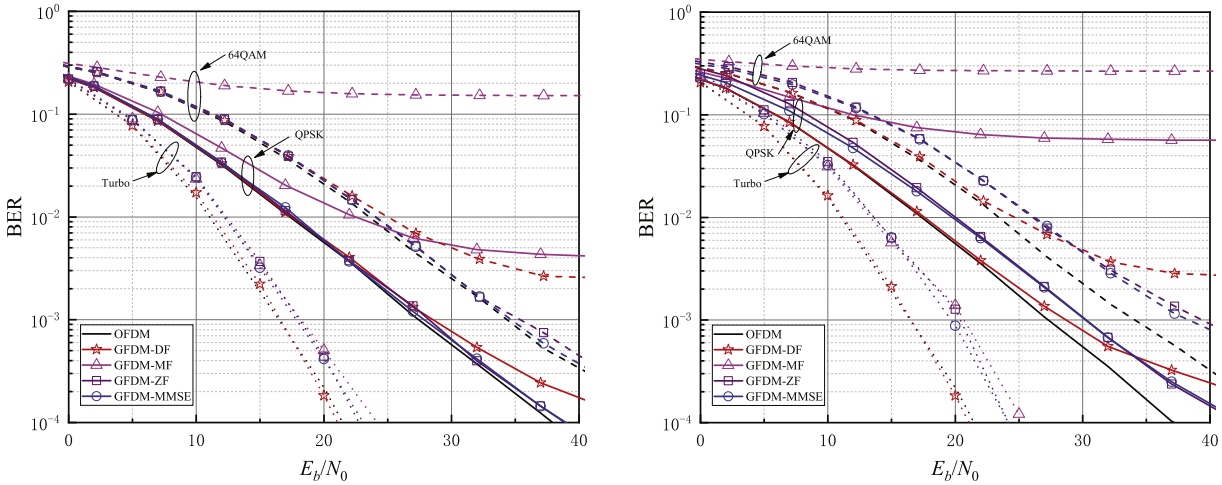

(a) $M = 7, K = 128$, and $\alpha = 0.25$ (b) $M = 7, K = 128$, and $\alpha = 0.75$

Fig. 8. BER performance comparison in Rayleigh channel with LS channel estimation. (a) $M = 7, K = 128$, and $\alpha = 0.25$. (b) $M = 7, K = 128$, and $\alpha = 0.75$.

64QAM. The reason is that GFDM-DF only adopts MF receiver, which without any treatment on the ISI. However, when Turbo coding is available, GFDM-DF can still achieve the same performance as OFDM.

3) MSE: Fig. 9 also illustrates the MSE of LS CE over EPA and Rayleigh channel with $\alpha = 0.75$ [38]. The MSE performance of GFDM-DF scheme is better than the conventional GFDM no matter in either EPA or Rayleigh channel. The curve of GFDM-DF scheme is consistent with the OFDM system in the low SNR region. When in the high SNR region, due to the influence of ISI, the performance of GFDM-DF is worse than OFDM especially in the Rayleigh fading channel.

C. Performance Comparison of SFBC for GFDM-DF Scheme

Fig. 10(a) shows that the BER performance of SFBC-GFDM-DF scheme is close to the SFBC-OFDM system in EPA channel. But the conventional SFBC-GFDM system cannot show a similar result even using ideal CE. The performance of SFBC-GFDM-MF receiver leads to a stronger degradation, and the SFBC-GFDM-ZF receiver suffers from a performance loss of 3 dB at BER=10^{-3}, the SFBC-GFDM-MMSE receiver has a performance loss of 1.7 dB at BER=10^{-3}. In Fig. 10(b), Rayleigh fading channel is applied, GFDM-DF suffers from severe ISI, which results in performance degradation compared with OFDM. However the performance is still better than conventional GFDM.

D. Complexity Analysis

The number of multiplications of the different GFDM receiver is described in Table III.

In GFDM-MF, the receiver matrix is a Hermitian conjugate of the transmitter matrix $\mathbf{A}$. In GFDM-ZF, the receiver matrix is a generalized inverse matrix of the transmitter matrix $\mathbf{A}$. Since ZF receiver matrix does not involve the channel coefficient, the receiving matrix can be stored in advance. Therefore, the GFDM-MF and GFDM-ZF receiver methods require $(MK)^2$ complex multiplications (CMs). The GFDM-MMSE needs to reconstruct the receiver matrix for different SNR, which has the

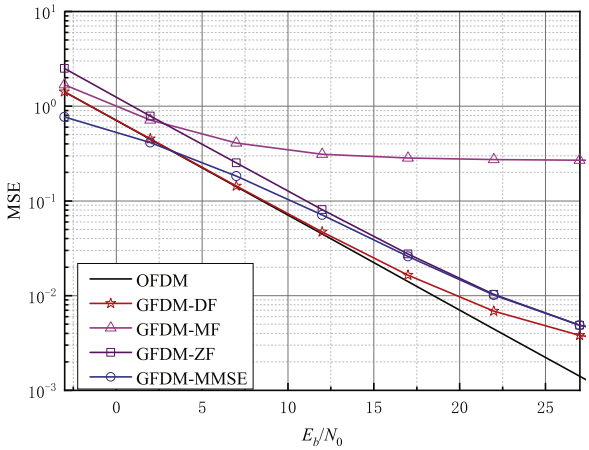

(a) EPA, $M = 7, K = 128$, and $\alpha = 0.75$

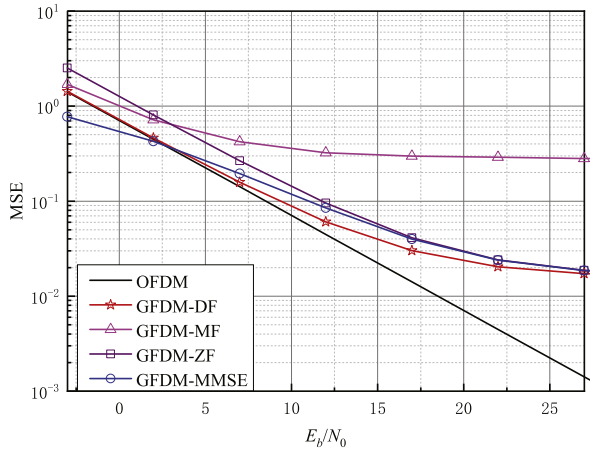

(b) Rayleigh, $M = 7, K = 128$, and $\alpha = 0.75$

Fig. 9. MSE performance comparison of channel estimation in EPA and Rayleigh channel. (a) $M = 7, K = 128$, and $\alpha = 0.25$. (b) $M = 7, K = 128$, and $\alpha = 0.75$.

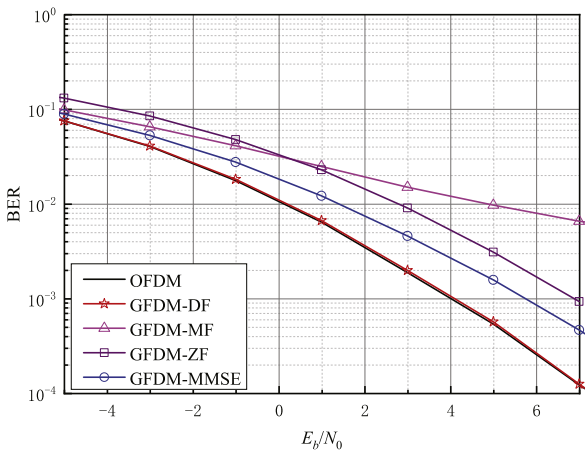

(a) EPA, $M = 7, K = 128$, and $\alpha = 0.75$

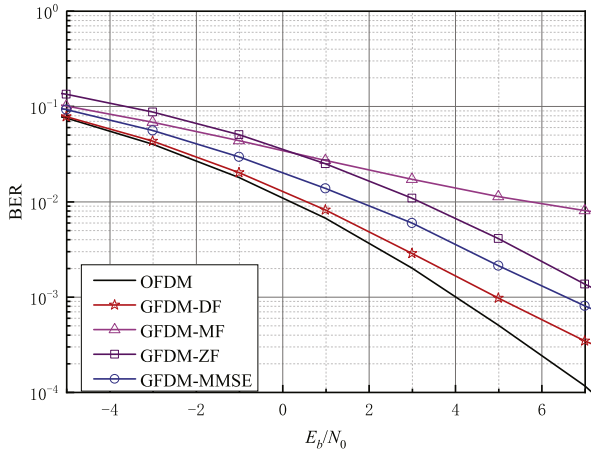

(b) Rayleigh, $M = 7, K = 128$, and $\alpha = 0.75$

Fig. 10. BER performance comparison of 2×2 MIMO in EPA and Rayleigh channel with ideal channel estimation. (a) $M = 7, K = 128$, and $\alpha = 0.25$. (b) $M = 7, K = 128$, and $\alpha = 0.75$.

TABLE III
COMPLEXITY OF DIFFERENT GFDM RECEIVERS

Techniques	Number of Multiplications
GFDM-MF	$(MK)^2$
GFDM-ZF	$(MK)^2$
GFDM-MMSE	$\frac{4}{3}(MK)^3 + (MK)^2$
GFDM-DF	$(MK)^2$
GFDM-DF-Low	$\frac{1}{2}MK\log_2(MK)+$ $MK^2 + \frac{1}{2}MK\log_2(\frac{MK}{2})$
GFDM-MF-SIC in [13]	$(MK)^2 + 2K(MK)^2$
GFDM-OQAM in [14]	$2(MK)^2$
GFDM-FFT in [39]	$\frac{KM}{2}\log_2 M + KLM + \frac{MK}{2}\log_2 MK$

complexity of $o\left(M^3K^3\right)$ CMs [40]. The computational complexity of GFDM-MMSE is about $\frac{4}{3}(MK)^3 + (MK)^2$ CMs.

It can be seen from equations (20), (25) and (26), the GFDM-DF receiver has two matrices. However, the dimensions of each matrix are only half that of conventional GFDM. So the computational complexity of GFDM-DF is the same as conventional GFDM. In the low complexity receiver of GFDM-DF, the receiving matrix is divided into M small matrices, which simplifies the computational complexity.

The complexity of different GFDM receiver techniques is evaluated in Fig. 11. The proposed GFDM-DF has the same computational complexity as GFDM-MF and GFDM-ZF receiver. Compared with GFDM-OQAM [14], GFDM-DF can reduce two times computational complexity. The complexity of GFDM-MMSE and GFDM-MF-SIC is too high when compared with the proposed GFDM-DF. GFDM-DF-Low has almost the same computational complexity as GFDM-FFT. Compared to the GFDM-DF, the computational complexity of GFDM-DF-Low can be significantly reduced as M increases. Therefore, the low complexity approach is more suitable for the case where there are fewer sub-carriers and larger sub-symbols in a GFDM block.

E. Power Spectral Density

The comparison of power spectral density (PSD) for OFDM, GFDM-DF and conventional GFDM is illustrated in Fig. (12).

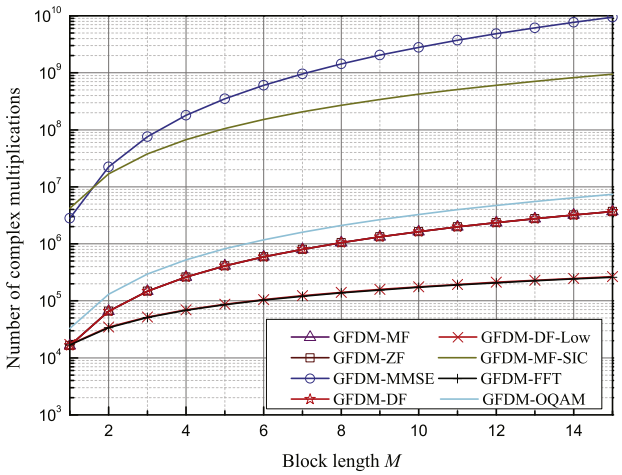

Fig. 11. Complexity comparison of different GFDM receivers.

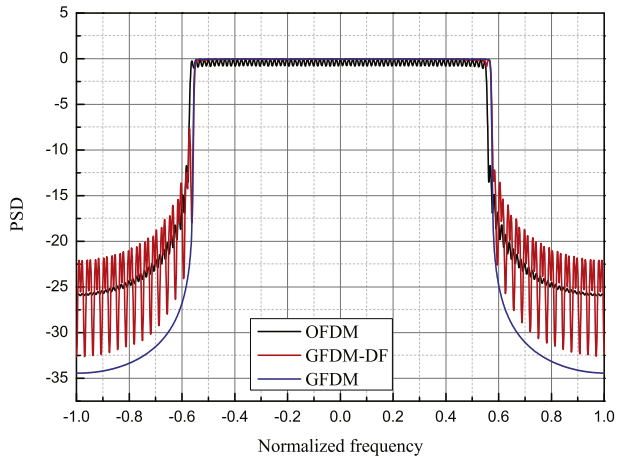

Fig. 12. PSD comparison between OFDM, GFDM-DF, and GFDM.

It can be seen that the OOB radiation of conventional GFDM is lower than OFDM. However, the proposed GFDM-DF scheme has an unsatisfactory performance, whose OOB radiation is even higher than OFDM. The reason for this phenomenon is mainly due to the design of the filter. The filter g^{e} and g^{o} are used on even-numbered and odd-numbered sub-carriers, respectively. However, the impulse response of g^{o} is discontinuous in the time domain, which leads to a higher OOB radiation.

VIII. Conclusion

In this paper, a new GFDM-DF transceiver with dual-filter was proposed. By applying different filters on even-numbered and odd-numbered sub-carriers to eliminate the interference between adjacent sub-carriers, the SIR of the GFDM-DF scheme can be greatly improved. Compared with conventional GFDM, GFDM-DF selects a large roll-off factor α, which can not only decrease the implementation complexity but also has no effect on the BER performance. Moreover, a larger roll-off factor can also make the symbol a better time-frequency localization, which is able to reduce the effect of time-offset on BER performance. Thus, when under a less severe channel, the proposed GFDM-DF can almost achieve the same BER performance as OFDM. In addition, GFDM-DF can work properly under the channel estimation and be easily combined with SFBC. Although GFDM-DF eliminates the ICI, it is still affected by ISI, and therefore the performance of GFDM-DF is worse than that of OFDM under a severe channel. This is a problem that needs solving in the next step.

References

[1] F. Li, L. Zhao, K. Zheng, and J. Wang, "A interference-free transmission scheme for GFDM system," in *Proc. IEEE Globecom Workshops*, Dec. 2016, pp. 1–6.
[2] J. A. C. Bingham, "Multicarrier modulation for data transmission: An idea whose time has come," *IEEE Commun. Mag.*, vol. 28, no. 5, pp. 5–14, May 1990.
[3] S. Chen and J. Zhao, "The requirements, challenges, and technologies for 5G of terrestrial mobile telecommunication," *IEEE Commun. Mag.*, vol. 52, no. 5, pp. 36–43, May 2014.
[4] M. Mirahmadi, A. Al-Dweik, and A. Shami, "BER reduction of OFDM based broadband communication systems over multipath channels with impulsive noise," *IEEE Trans. Commun.*, vol. 61, no. 11, pp. 4602–4615, Nov. 2013.
[5] S. A. Fechtel and A. Blaickner, "Efficient FFT and equalizer implementation for OFDM receivers," *IEEE Trans. Consum. Electron.*, vol. 45, no. 4, pp. 1104–1107, Nov. 1999.
[6] P. Banelli, S. Buzzi, G. Colavolpe, A. Modenini, F. Rusek, and A. Ugolini, "Modulation formats and waveforms for 5G networks: Who will be the heir of OFDM?: An overview of alternative modulation schemes for improved spectral efficiency," *IEEE Signal Process. Mag.*, vol. 31, no. 6, pp. 80–93, Nov. 2014.
[7] G. Wunder *et al.*, "5GNOW: Non-orthogonal, asynchronous waveforms for future mobile applications," *IEEE Commun. Mag.*, vol. 52, no. 2, pp. 97–105, Feb. 2014.
[8] M. Matth, N. Michailow, I. Gaspar, and G. Fettweis, "Influence of pulse shaping on bit error rate performance and out of band radiation of generalized frequency division multiplexing," in *Proc. IEEE Int. Conf. Commun. Workshops*, Jun. 2014, pp. 43–48.
[9] G. Fettweis, M. Krondorf, and S. Bittner, "GFDM—Generalized frequency division multiplexing," in *Proc. 69th IEEE Veh. Technol. Conf.*, Apr. 2009, pp. 1–4.
[10] M. Danneberg, R. Datta, and G. Fettweis, "Experimental testbed for dynamic spectrum access and sensing of 5G GFDM waveforms," in *Proc. 80th IEEE Veh. Technol. Conf.*, Sep. 2014, pp. 1–5.
[11] N. Michailow and G. Fettweis, "Low peak-to-average power ratio for next generation cellular systems with generalized frequency division multiplexing," in *Proc. Int. Symp. Intell. Signal Process. Commun. Syst.*, Nov. 2013, pp. 651–655.
[12] A. RezazadehReyhani, A. Farhang, and B. Farhang-Boroujeny, "Circularly pulse-shaped waveforms for 5G: Options and comparisons," in *Proc. IEEE Global Commun. Conf.*, Dec. 2015, pp. 1–7.
[13] R. Datta, N. Michailow, M. Lentmaier, and G. Fettweis, "GFDM interference cancellation for flexible cognitive radio PHY design," in *Proc. IEEE Veh. Technol. Conf.*, Sep. 2012, pp. 1–5.
[14] I. Gaspar, M. Matth, N. Michailow, L. L. Mendes, D. Zhang, and G. Fettweis, "Frequency-shift offset-QAM for GFDM," *IEEE Commun. Lett.*, vol. 19, no. 8, pp. 1454–1457, Aug. 2015.
[15] G. Taricco and E. Biglieri, "Space-time decoding with imperfect channel estimation," *IEEE Trans. Wireless Commun.*, vol. 4, no. 4, pp. 1874–1888, Jul. 2005.
[16] M. Biguesh and A. B. Gershman, "MIMO channel estimation: Optimal training and tradeoffs between estimation techniques," in *Proc. IEEE Int. Conf. Commun.*, Jun. 2004, pp. 2658–2662.
[17] S. Coleri, M. Ergen, A. Puri, and A. Bahai, "Channel estimation techniques based on pilot arrangement in OFDM systems," *IEEE Trans. Broadcast.*, vol. 48, no. 3, pp. 223–229, Sep. 2002.
[18] S. Ehsanfar, M. Matthe, D. Zhang, and G. Fettweis, "Theoretical analysis and CRLB evaluation for pilot-aided channel estimation in GFDM," in *Proc. IEEE Global Commun. Conf.*, Dec. 2016, pp. 1–7.
[19] J. Du, "Pulse shape adaptation and channel estimation in generalised frequency division multiplexing systems," Ph.D. dissertation, School Inf. Commun. Technol., KTH Roy. Inst. Technol., Stockholm, Sweden, 2008.
[20] S. Ehsanfar, M. Matthe, D. Zhang, and G. Fettweis, "Interference-free pilots insertion for MIMO-GFDM channel estimation," in *Proc. IEEE Wireless Commun. Netw. Conf.*, Mar. 2017, pp. 1–6.

[21] U. Vilaipornsawai and M. Jia, "Scattered-pilot channel estimation for GFDM," in *Proc. IEEE Wireless Commun. Netw. Conf.*, Apr. 2014, pp. 1053–1058.
[22] K. F. Lee and D. B. Williams, "A space-time coded transmitter diversity technique for frequency selective fading channels," in *Proc. IEEE Sensor Array Multichannel Signal Process. Workshop*, Mar. 2000, pp. 149–152.
[23] N. Al-Dhahir, "Single-carrier frequency-domain equalization for space-time block-coded transmissions over frequency-selective fading channels," *IEEE Commun. Lett.*, vol. 5, no. 7, pp. 304–306, Jul. 2001.
[24] N. Michailow *et al.*, "Generalized frequency division multiplexing for 5th generation cellular networks," *IEEE Trans. Commun.*, vol. 62, no. 9, pp. 3045–3061, Sep. 2014.
[25] M. Matthe, L. L. Mendes, and G. Fettweis, "Space-time coding for generalized frequency division multiplexing," in *Proc. 20th Eur. Wireless Conf.*, May. 2014, pp. 1–5.
[26] N. Michailow, L. Mendes, M. Matth, I. Gaspar, A. Festag, and G. Fettweis, "Robust WHT-GFDM for the next generation of wireless networks," *IEEE Commun. Lett.*, vol. 19, no. 1, pp. 106–109, Jan. 2015.
[27] M. Matth, L. L. Mendes, and G. Fettweis, "Generalized frequency division multiplexing in a Gabor transform setting," *IEEE Commun. Lett.*, vol. 18, no. 8, pp. 1379–1382, Aug. 2014.
[28] N. Michailow, S. Krone, M. Lentmaier, and G. Fettweis, "Bit error rate performance of generalized frequency division multiplexing," in *Proc. IEEE Veh. Technol. Conf.*, Sep. 2012, pp. 1–5.
[29] C. Kim, K. Kim, Y. H. Yun, Z. Ho, B. Lee, and J. Y. Seol, "QAM-FBMC: A new multi-carrier system for post-OFDM wireless communications," in *Proc. IEEE Global Commun. Conf.*, Dec. 2015, pp. 1–6.
[30] H. Nam, M. Choi, C. Kim, D. Hong, and S. Choi, "A new filter-bank multicarrier system for QAM signal transmission and reception," in *Proc. IEEE Int. Conf. Commun.*, Jun. 2014, pp. 5227–5232.
[31] N. Michailow, R. Datta, S. Krone, M. Lentmaier, and G. Fettweis, "Generalized frequency division multiplexing: A flexible multi-carrier modulation scheme for 5th generation cellular networks," in *Proc. German Microw. Conf.*, vol. 62, 2012, pp. 1–4.
[32] H. Nam, M. Choi, S. Han, C. Kim, S. Choi, and D. Hong, "A new filter-bank multicarrier system with two prototype filters for QAM symbols transmission and reception," *IEEE Trans. Wireless Commun.*, vol. 15, no. 9, pp. 5998–6009, Sep. 2016.
[33] K. Zheng, F. Liu, L. Lei, C. Lin, and Y. Jiang, "Stochastic performance analysis of a wireless finite-state Markov channel," *IEEE Trans. Wireless Commun.*, vol. 12, no. 2, pp. 782–793, Feb. 2013.
[34] S. M. Alamouti, "A simple transmit diversity technique for wireless communications," *IEEE J. Sel. Areas Commun.*, vol. 16, no. 8, pp. 1451–1458, Oct. 1998.
[35] X. Yang and B. Vucetic, "A frequency domain multi-user detector for TD-CDMA systems," *IEEE Trans. Commun.*, vol. 59, no. 9, pp. 2424–2433, Sep. 2011.
[36] K. Zheng, H. Meng, P. Chatzimisios, L. Lei, and X. Shen, "An SMDP-based resource allocation in vehicular cloud computing systems," *IEEE Trans. Ind. Electron.*, vol. 62, no. 12, pp. 7920–7928, Dec. 2015.
[37] "Multiplexing and channel coding (release 14)," 3GPP, Sophia Antipolis, France, TS 36.212 V14.4.0, Sep. 2017.
[38] L. Lei, Y. Zhang, X. S. Shen, C. Lin, and Z. Zhong, "Performance analysis of device-to-device communications with dynamic interference using stochastic Petri Nets," *IEEE Trans. Wireless Commun.*, vol. 12, no. 12, pp. 6121–6141, Dec. 2013.
[39] N. Michailow, I. Gaspar, S. Krone, M. Lentmaier, and G. Fettweis, "Generalized frequency division multiplexing: Analysis of an alternative multi-carrier technique for next generation cellular systems," in *Proc. Int. Symp. Wireless Commun. Syst.*, Aug. 2012, pp. 171–175.
[40] A. Farhang, N. Marchetti, and L. E. Doyle, "Low-complexity modem design for GFDM," *IEEE Trans. Signal Process.*, vol. 64, no. 6, pp. 1507–1518, Mar. 2016.

Fei Li (S'18) received the M.S. degree in electronics engineering from Inner Mongolia University, Hohhot, China, in 2014. He is currently working toward the Ph.D. degree with the Intelligent Computing and Communication Lab, Key Lab of Universal Wireless Communications, Ministry of Education, Beijing University of Posts and Telecommunications, Beijing, China. His research interest include 5G wireless communications, such as new waveform and channel estimation, etc.

Kan Zheng (SM'09) received the B.S., M.S., and Ph.D. degrees from the Beijing University of Posts and Telecommunications (BUPT), Beijing, China, in 1996, 2000, and 2005, respectively. He is currently a Full Professor with the BUPT. He is the author of more than 200 journal and conference papers in the field of wireless networks, Internet-of-Things, etc. He holds Editorial Board positions for several journals. He has rich experiences on the research and standardization of new emerging technologies. He is currently a Chair of the IEEE Computer Society Special Technical Communities Internet-of-Everything. He has also served in the Organizing/Technical Program Committees for more than ten conferences such as IEEE International Symposium on Personal, Indoor and Mobile Radio Communications, IEEE SmartGrid, etc.

Long Zhao (M'17) received the Ph.D. degree from the Beijing University of Posts and Telecommunications (BUPT), Beijing, China, in 2015. From April 2014 to March 2015, he was a Visiting Scholar with the Department of Electrical Engineering, Columbia University, New York, NY, USA. He is currently an Associate Professor with BUPT. His research interests include wireless communications and signal processing.

Hui Zhao received the M.S. degree in 2003 from Tianjin University, Tianjin, China, and the Ph.D. degree in 2006 from the Beijing University of Posts and Telecommunications (BUPT), Beijing, China. She is currently an Associate Professor with the BUPT. She has accumulated rich experience in the field of LTE-Advanced, ultra-high throughput WLAN, and 5G. Till now, she has authored/coauthored more than 80 papers in the journals and conferences and holds 18 authorized patents.

Yonghui Li (M'04–SM'09–F'19) received the Ph.D. degree from the Beijing University of Aeronautics and Astronautics, Beijing, China, in 2002. From 1999 to 2003, he was with Linkair Communication Inc., where he held a position of Project Manager with responsibility for the design of Physical Layer solutions for the LAS-CDMA system. Since 2003, he has been with the Centre of Excellence in Telecommunications, the University of Sydney, Sydney, NSW, Australia, where he is currently a Professor with the School of Electrical and Information Engineering. He is the recipient of the Australian Queen Elizabeth II Fellowship in 2008 and the Australian Future Fellowship in 2012. He holds a number of patents granted and pending in the field of wireless communications, with a particular focus on MIMO, millimeter wave communications, machine to machine communications, coding techniques, and cooperative communications. He is now an Editor for the IEEE TRANSACTIONS ON COMMUNICATIONS and IEEE TRANSACTIONS ON VEHICULAR TECHNOLOGY. He was a Guest Editor for several special issues of IEEE journals, such as IEEE JOURNAL ON SELECTED AREAS IN COMMUNICATIONS special issue on Millimeter Wave Communications. He received the best paper awards from IEEE International Conference on Communications 2014, IEEE International Symposium on Personal, Indoor and Mobile Radio Communications 2017, and IEEE Wireless Days Conferences 2014.